Optical Single Sideband Modulation Using a Semiconductor Laser under Modulated Light Injection

Hye-Seung Ryu

The Graduate School

Yonsei University

Department of Electrical and Electronic Engineering

Optical Single Sideband Modulation

Using a Semiconductor Laser

under Modulated Light Injection

A Master's Thesis

Submitted to the Department of Electrical and Electronic Engineering

and the Graduate School of Yonsei University

in partial fulfillment of the requirements for the degree of

Master of Science

Hye-Seung Ryu

January 2004

This certifies that the master's thesis of [Hye-Seung Ryu] is approved.

———————————————

Thesis Supervisor: [Woo-Young Choi]

———————————————

[Ilgu Yun]

———————————————

[Sangin Kim]

The Graduate School

Yonsei University

January 2004

Index

Figure Index

Table Index

Abstract

Optical Single Sideband Modulation using a Semiconductor Laser under Modulated Light Injection

Ryu, Hye-Seung

Dept. of Electrical and Electronic Eng.

The Graduate School

Yonsei University

The new optical single sideband (OSSB) modulation technique that overcomes modulation bandwidth limitation and chromatic dispersion effect simultaneously is proposed and successfully demonstrated. The new scheme simply uses an additional standard semiconductor laser as an active optical filter for the input modulated signals.

From the numerical analysis of optical injection locking, it is shown that the slave laser (SL) injected by a single mode master laser (ML) has all the power at the frequency of the ML within locking range, determined by frequency difference and power ratio between the ML and the SL. In addition, from the theoretical and experimental analysis for the SL under injections

from several MLs, it is found that the SL has its power distributed at the frequencies of the MLs within the estimated locking range and the larger power is emitted at the lower frequency (or longer wavelength) among them. From the power relationship of the input MLs and output SL, it can be considered that the SL has the wavelength selective amplification characteristics.

Based on the wavelength selective amplification characteristics of the SL under external light injection, the SL suppresses an unselected sideband of the input double sideband signals to generate single sideband signal and amplifies the other sideband to improve modulation response effectively. In addition, since the SL suppresses the excess optical carrier as well as enhances the selected sideband, increased optical modulation depth can be obtained.

ix

I. Introduction

Radio-on-fiber (RoF) systems have attracted attentions for the future cellular radio access networks such as mobile communication; roadside-to-vehicle radio access links in intelligent transportation system; and indoor wireless LAN [1]. This is mainly because the RoF systems transmit the microwave and millimeter-wave (MW) signals from the central office to base stations through optical fibers having low loss, large bandwidth and immunity to electromagnetic interference. A simple and cost-effective approach to transmit MW signals over the favorable optical fibers is to employ intensity modulation, which modulates laser diode directly at MW frequency or modulate CW signal from laser diode with external modulator at MW frequency. In the intensity modulations, there are two issues that have been intensively researched: modulation bandwidth limitation and chromatic dispersion induced detected power degradation.

First, the modulation bandwidth of the intensity modulation is limited by that of semiconductor lasers and external modulators. For the semiconductor laser, the modulation bandwidth is limited by its photon-electron resonance frequency, so it is hard to achieve modulation bandwidth over a few tens of gigahertz at room temperature [2]. For the external modulator, modulation bandwidth is also inherently limited by its RC

constant, structure, and materials.

Another issue in intensity modulation is the detected power degradation due to chromatic dispersion of optical fibers. The intensity modulated signals have two sidebands separated by the desired microwave or millimeter-wave frequency f_{MW} from the optical carrier in the optical spectrum, which is so called double sideband (DSB) signal. As they propagate through the dispersive optical fibers, two sideband signals experience disparate phase-shifts because they travel in different velocities owing to fiber chromatic dispersion. Whenever the relative phase difference between two sidebands becomes π, the photo-detected signal powers are greatly suppressed.

In this thesis, a novel optical single sideband modulation scheme overcoming not only dispersion induced detected power degradation but also limited modulation bandwidth is proposed and demonstrated. A semiconductor under intensity modulated light injection is used as an active optical filter, which gives gain to weakly modulated sideband and filter our undesired sideband. First, Section II introduces the previous methods to solve the two problems in intensity modulation. Then, Section III and IV show the origins of the proposed scheme, which are the wavelength selective amplification characteristics of the semiconductor laser under light injection depending on injection level and frequency detuning. Section III deals with locking condition, locked power characteristics, and stability properties for

an injection locked semiconductor laser to a single mode diode laser. In Section IV, the properties of an SL subject to external light injection from several lasers are investigated based on numerical analysis and experiments. Section V is devoted to the proposed scheme based on the experiments and simulations. Finally, section VI concludes this thesis.

II. Review of the previous methods

As mentioned before, since the modulation bandwidth limitation and the chromatic dispersion induced detected power degradation have been attractive research topics; there exist various methods for overcoming each problem. Therefore, this section reviews the previous notable methods in two parts: modulation bandwidth enhancement and optical single sideband modulation for overcoming chromatic dispersion effect.

A. Modulation bandwidth enhancement methods

A.1) Direct modulation

The typical approach to enhance modulation bandwidth is to fabricate the high speed semiconductor laser using new materials and structures. For example, 33GHz GaAs-based pseudomorphic multiple-quantum-well (MQW) ridge-waveguide lasers [3] and 40GHz undoped short-cavity $In_{0.35}Ga_{0.65}As$-GaAs MQW lasers [4] have been reported. However, these usually result in more complex fabrication processes and increased costs. Therefore, other approaches using standard semiconductor lasers have been proposed.

One is to increase the modulation bandwidth directly by changing internal characteristics of the laser diodes. For example, using the strong light injection, the injection-locked laser obtains larger resonance frequency and the available 3dB modulation bandwidth [5, 7]. The modulation bandwidth is limited by the electron-photon resonance frequency ω_p, which can be approximated by [6]

$$\omega_p = \sqrt{\frac{g_o S_o}{\tau_p (1 + \varepsilon S_o)}} \tag{2.1}$$

where g_o is the differential gain, S_o the mean photon density, τ_p the photon life time, and ε the gain compression factor. Under proper locking condition, as the external laser optical field is coherently added to the slave laser optical filed, the injected laser has higher resonance frequency and modulation bandwidth [7]. The recent paper reported that the modulation bandwidth was enhanced by as much as 3.7 times using strong injection locking [5].

The other is to enhance modulation bandwidth effectively by increasing harmonic signals of the laser diodes. Since the modulation bandwidth limitation bring about the weak RF power at higher frequency, enhancing the weak high frequency harmonic signals can be interpreted as the modulation

bandwidth enhancement. As an example of this method, external feedback effectively enhances the desired harmonic content generated by large-signal modulation, as the cavity filters out unwanted frequency components [8]. The paper demonstrated fourth harmonic at 5GHz [8].

A.2) External modulation

For external modulation, likewise direct modulation, researches have been performed to increase the modulation bandwidth of the external modulator in the level of device fabrications. For example, the external electro-absorption modulator with narrow mesa ridge waveguide has had 40 GHz speed [9], 110 GHz polymer modulator has been reported [10], and 40 GHz traveling-wave electro-absorption modulator has been demonstrated [11]. These also require complex fabrication processes and high costs. Therefore, harmonic generation, which uses the inherent nonlinearity of modulators, is a promising alternative to the methods above, because relatively cheap, lower frequency components can be used. For example, harmonic generation using MZ modulator has been used to give a modulated signal at 36 GHz [12]. Using the steep nonlinear absorption characteristics of the electroabsorption modulators provides benefits of suitability for integration with DFB lasers and their low drive voltage requirement [13].

B. Optical single sideband modulation methods

As mentioned before, the chromatic dispersion induced detected power degradation is mainly because the intensity modulated signal has two sidebands, which experience different optical phases over optical fibers. Therefore, one of the sidebands is required to be eliminated, and various single sideband (SSB) modulation techniques have been demonstrated. Optical sideband filtering using fiber Bragg grating is simple but requires a filter with very narrow optical passband and high reflectivity [14]. Dual electrode Mach-Zehnder electro-optic modulators can be utilized for optical SSB modulation, but its operation is sensitive to bias phase shifts [15]. The optical single-sideband suppressed-carrier modulation has been performed using a standard single-electrode Mach-Zehnder electrooptic modulator (MZ-EOM) bidirectionally [16]. This method has advantage of being independent on the MZ-EOM bias, but it is required to center the modulator's location precisely within the Sagnac loop.

The above reviews show that the previous methods have successfully demonstrated. However, there is still need for the new solutions to solve the two problems simultaneously. Therefore, this thesis proposes the new optical single sideband modulation overcoming both modulation bandwidth limitation and chromatic dispersion effect at the same time. From the next

section dealing with the origins of the proposed scheme, all the discussion

focused on the new method.

III. Characteristics of Injection-Locked Semiconductor Laser

A. Theory
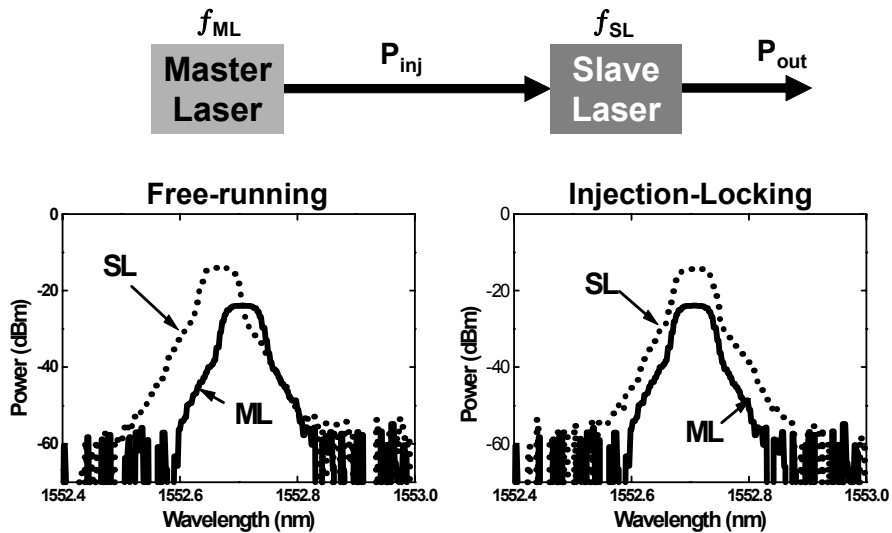
Figure 3.1 Optical injection locking configuration.

Optical injection locking is a way of synchronizing one (or several) free-running slave laser (SL) to a stabilized master laser (ML) under the proper condition of power ratio (P_{inj}/P_{out}) and differences ($\Delta f = f_{ML} - f_{SL}$) in lasing frequency (or wavelength) between the two lasers. In order to investigate the properties of injection-locked

semiconductor laser, it is considered that light from an ML is injected into an SL, as shown in Fig. 3.1. The two semiconductor lasers emit in a single longitudinal mode and with a very small difference in frequency (or wavelength). The numerical analysis is based on the following modified rate equations for the complex electric field of the SL [17]:

$$\frac{d}{dt}E_{SL}(t) - \left\{ j\omega(N) + \frac{1}{2}\left[G(N) - \frac{1}{\tau_p} \right] \right\} E_{SL}(t) = \eta f_d E_{ML}(t) \qquad (3.1)$$

This equation is derived from a traveling wave description of the field inside laser cavity. In the equation, $E_{SL}(t)$ and $E_{ML}(t)$ are the SL and ML electric field, which are represented by [17]

$$E_{SL}(t) = E_0(t) e^{j[\omega_0 t + \phi_0(t)]} \qquad (3.2)$$

$$\eta E_{ML}(t) = E_1 e^{j[\omega_1 t + \phi_1]} \qquad (3.3)$$

where $E_0(t)$, E_1, $\phi_0(t)$, and ϕ_1 are real-valued and ω_0 is the angular oscillation frequency of SL without injected signal; $\omega(N)$ and $G(N)$ the angular optical frequency and the modal gain per second of the SL, respectively; τ_p the photon lifetime; f_d the longitudinal mode spacing; and η the coupling efficiency. Since the master laser is intended to be a

stabilized source, the phase noise can be neglected.

Through the Eq. 3.2, Eq. 3.3, assuming that $G(N)$ is a linear function of carrier density, and the carrier density dependent angular optical frequency of the SL, Eq. 3.1 can be transformed to the amplitude-phase representation

$$\frac{d}{dt}E_0(t) = \frac{1}{2}G_N\Delta N(t)E_0(t) + f_d E_1 \cos(\Delta(t)) \tag{3.4}$$

$$\frac{d}{dt}\phi_0(t) = \frac{1}{2}\alpha G_N\Delta N(t) + f_d \frac{E_1}{E_0(t)}\sin(\Delta(t)) \tag{3.5}$$

$$\frac{d}{dt}N(t) = J - \frac{N(t)}{\tau_s} - G(N)E_0^2(t) \tag{3.6}$$

where the α is the linewidth enhancement factor, the photon density equals the squared amplitude of the electric field with the given normalization, J is the pumping term, and τ_s the spontaneous emission lifetime. Through the three Eqs. 3.4, 3.5, and 3.6, the basic theoretical model for the optical injection locking can be analyzed. In Eqs. 3.4 and 3.5

$$\Delta(t) = \Delta\omega t - \phi_0(t) \tag{3.7}$$

$$\Delta\omega = 2\pi\Delta f = \omega_1 - \omega_0 \tag{3.8}$$

In injection locked steady state, the maximum angular frequency

detuning between the master and the free-running slave yields [17]

$$\left|\Delta\omega\right| = \left|\omega_1 - \omega_0\right| \le f_d \frac{E_1}{\widetilde{E}_0} \sqrt{1+\alpha^2} \tag{3.9}$$

where $\widetilde{E}_0$ is the stationary value of $E(t)$ without injection.

In the static locking range, mainly two regimes can be distinguished: dynamically stable locking and unstable locking. When a small fluctuation is introduced, the SL within stable locking range (S) maintains locked state. On the other hand, the SL falling in unstable locking range (US) shows undamped relaxation oscillation and chaos. Such an oscillation and chaos produce multiple sidebands in the output spectra. In the static unlocking range (U) where the slave laser does not lock on the master laser, beating between the master and the slave fields inside the nonlinear slave laser medium leads to four-wave mixing and subharmonic generation [17-19].

Fig. 3.2 shows the locking range for the frequency detuning between the ML and SL as a function of injection power ratio. Small fluctuations δE, $\delta\phi$, and δN around the stationary solutions are applied to the three Eqs. 3.4, 3.5, and 3.6 and the first-order fluctuation terms are obtained. By the s-domain stability analysis of the obtained equations with the parameter listed in Table 1, the range for the stable locking regime can be determined. Here,

the injection level is defined as $\left(E_1/\widetilde{E}_0\right)^2$. The static locking range is determined by a given injection level, while the dynamic stable locking range is related to the frequency detuning between ML and SL. The stable locking range shows the asymmetric characteristics. The center of the stable-locking range is shifted toward the longer wave length of SL's lasing wavelength with increasing injection level.

Since the noticeable carrier density dependence of the refractive index of the gain medium significantly affects the injection locking properties in semiconductor laser, the locked output of the SL versus the detuning curve has a very asymmetric shape with respect to the optimum detuning [18]. Fig. 3.3 is the calculated locked output as the function of frequency detuning. The dark solid line and light solid line mean the dynamically stable parts and unstable parts, respectively. The asymmetric characteristics can be generally explained as the follows. If the SL output increases with the external light injection, the excited carrier density in the active region decreases correspondingly. Decreased carrier density leads to increase in the refractive index of the active region which results in the lowering of the cavity resonance frequency. Therefore the optimum locking can be achieved when the injected light frequency coincides with the resonance frequency which is downshifted by the light injection. This is related with the fact that the optical injection locking mechanism is stronger with the master at a longer

wavelength.
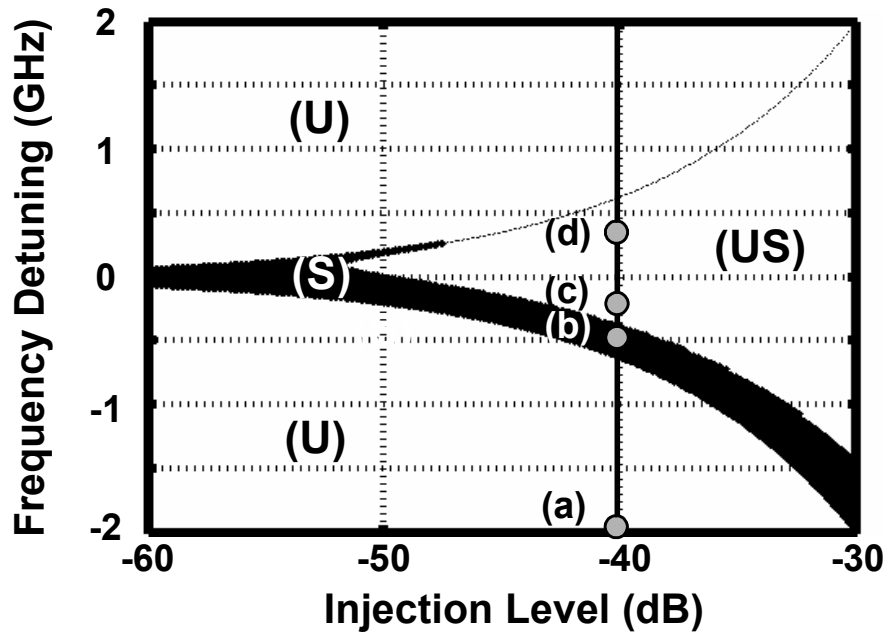
Figure 3.2 Locking characteristics as a function of injection level. S represents dynamically stable locking range; US dynamically unstable locking range; and U static unlocking range.
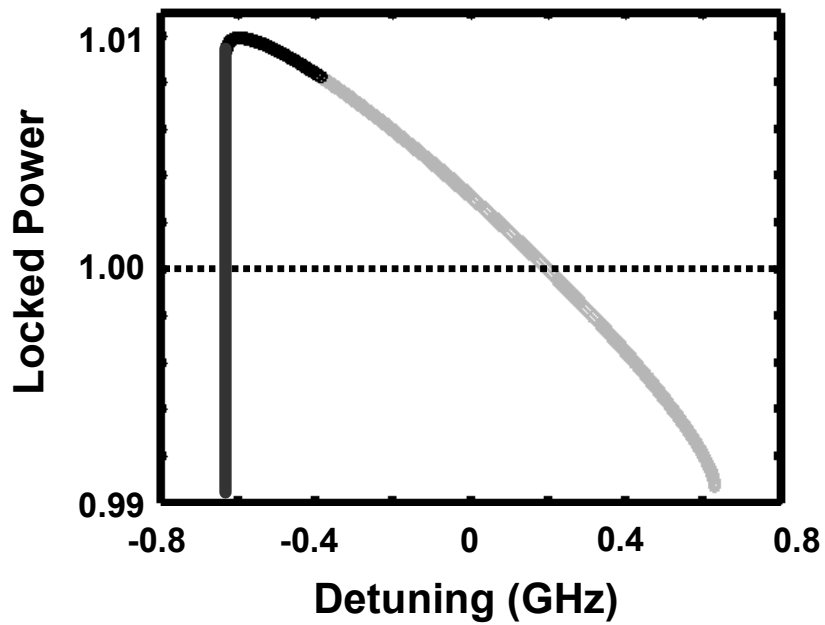
Figure 3.3 Locked power relative to free running power. Dark solid line and light solid line represent the dynamically stable locking states and unstable locking states, respectively

Table I. Laser Parameter and Their Numerical Values

Symbol	Parameter	Value
τ_s	Spontaneous emission lifetime	2ns
τ_p	Photon lifetime	2ps
f_d	Longitudinal mode spacing	125G GHz
G_N	Gain coefficient	$1.1 \times 10^{-11} \ m^3 s^{-1}$
N_0	Carrier density to reach zero gain	$1.1 \times 10^{24} \ m^{-3}$
α	Linewidth enhancement factor	3
I/I_{th}	Normalized bias current	1.3

B. Dynamic behavior

The SL transient responses under different locking conditions, as marked in Fig. 3.2 (a)-(d), can be solved by the fourth order Runge-Kutta integration of the OIL rate equation. Fig. 3.4 shows the power spectra for an injection level of -40dB and the different detuning conditions, which can be calculated using the fast Fourier transform of the solved steady-state SL transient response. In Fig. 3.4, the zero of the frequency axis in all cases corresponds to the ML frequency (Detuning$= f_{SL} - f_{ML}$).

First, Fig. 3.4 (a) is for the frequency detuning of $\Delta f = -2$ GHz in U regime. Since the SL is not locked to the ML, the SL's power spectra have large spectral component at the free-running SL frequency, noticeable component at the ML frequency, and a beat note on the other side of dominant line. With the interaction between ML and SL, the SL's lasing frequency is slightly shifted close to the ML's [14]. In Fig.3.4 (b) with $\Delta f =$ -500 MHz, stable locking is obtained so that all the power of the SL is concentrated at the ML frequency. Fig. 3.4 (c) and (d) in the dynamically unstable locked states show undamped relaxation oscillations. In Fig. 3.4 (c) with $\Delta f =$ -250 MHz, the locked main peak is dominant, but some power transfer to the relaxation oscillation sidebands. It shows sidebands only at the fundamental relaxation oscillation frequency of 2.5GHz. However,

approaching the upper limit of the full locking range, instability is stronger

and more harmonics is resulted as shown in Fig. 3.4 (d) with $\Delta f = 300$ MHz.
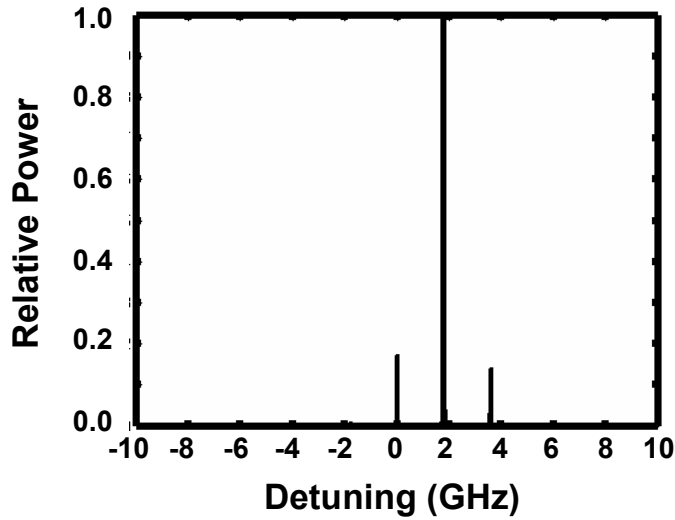
(a)
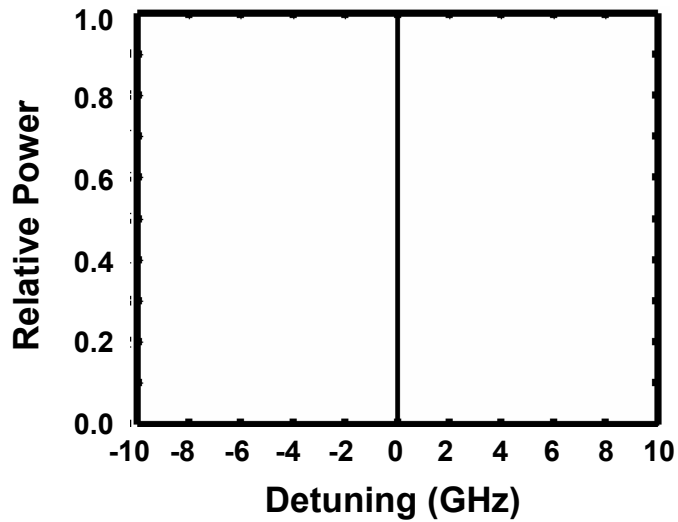
(b)

Figure 3.4 Power spectra for the different frequency detuning Δf at the

injection level of -40 dBm, corresponding to (a) ~ (d) in Fig. 3.2.
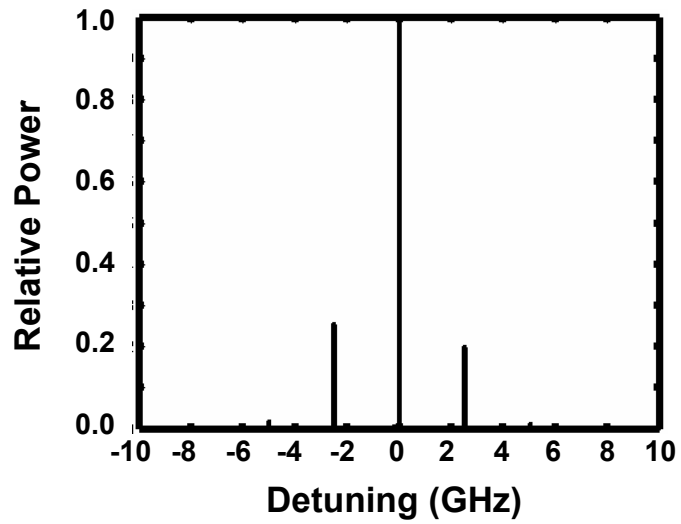
(c)
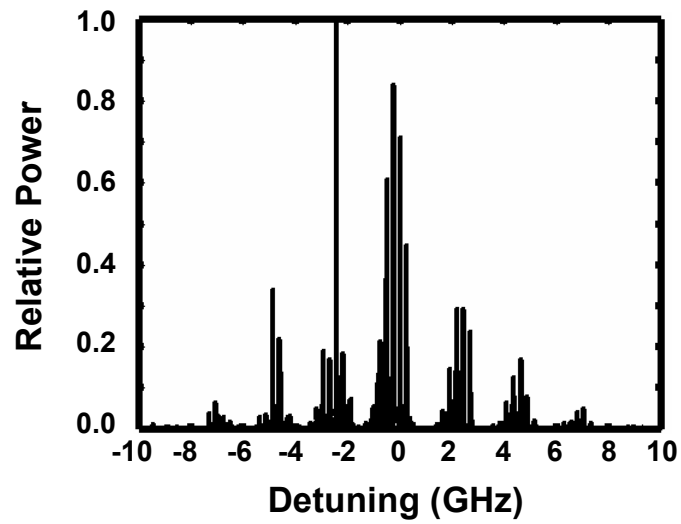
(d)

Figure 3.4 (continued)

IV. Characteristics of a semiconductor laser under external light injection from several lasers

The previous analysis on optical injection locking is focused on the synchronizing an SL to an ML using the rate-equation based model. In this section, the characteristics of an SL which is subject to light injection from several MLs are analyzed theoretically and experimentally.

A. Theory

The classical single master-slave injection-locking configuration is extended to take account of light injection from an arbitrary number of master lasers. The extended rate equation for the total complex electric field in the single-mode slave laser cavity under several master lasers can be written as

$$\frac{d}{dt}E_{SL}(t) - \left\{ j\omega(N) + \frac{1}{2}\left[G(N) - \frac{1}{\tau_p} \right] \right\}E_{SL}(t) = \eta f_d \sum_{m=1}^{l} E_{ML-m}(t) \qquad (4.1)$$

where $E_{ML-m}(t)$ is the complex electric field of master laser m, also inside the cavity of the slave laser [17, 20]. When dealing with two master lasers

and performing the same process in section III, the Eq. 4.1 can be converted

into the amplitude-phase representation such as

$$\frac{d}{dt}E_0(t) = \frac{1}{2}G_N \Delta N(t) E_0(t) + f_d E_1 \cos(\Delta_1(t)) + f_d E_2 \cos(\Delta_2(t)) \quad (4.2)$$

$$\frac{d}{dt}\phi_0(t) = \frac{1}{2}\alpha G_N \Delta N(t) + f_d \frac{E_1}{E_0(t)}\sin(\Delta_1(t)) + f_d \frac{E_2}{E_0(t)}\sin(\Delta_2(t)) \quad (4.3)$$

$$\frac{d}{dt}N(t) = J - \frac{N(t)}{\tau_s} - G(N)E_0^2(t) \quad (4.4)$$

Since the locking mechanism is usually considered when one SL is

locked to one ML, whether an SL can be locked to several independent MLs

at the same time or not is a tricky issue. Thus, here, it is impossible to define

the locking range for both MLs. However, the dynamic behavior of the SL

under several MLs is affected by the locking mechanism [20]. In order to

verify this, two MLs (M1 and M2) with the same power ($E_1 = E_2$) and

independent detuning frequency are considered. Since the amplitudes of the

MLs are equal, the calculated locking range of the SL for each ML is

identical. The dynamic behavior is examined with the approximated locking

range effectively. Even though the approximated locking range cannot

provide the accurate numerical analysis, it can give important clues for the

understanding of the SL's dynamic behavior related to locking mechanism.

Based on this locking range, the dynamic behavior of the SL is examined by

varying the detuning frequency of each ML.

In order to investigate the dynamic behavior of the SL under the two MLs, the power spectra is calculated based on the model Eqs. 4.2, 4.3, and 4.4, as shown in Fig.4.1. We used the same parameter as in section III except one, bias current condition ($I/I_{th} = 3$). The horizontal axis denotes the frequency shift between the ML and the free-running SL (the free-running SL frequency is the reference, $\Delta f = f_{ML} - f_{SL}$), whereas the vertical axis indicates the spectral density on a linear scale.

The situation in Fig. 4.1 (a) and (c) illustrates typical locking behavior. The SL is injection locked to only M1 within locking range of the SL. As expected from section III, the M1 mode locking the SL becomes the largest spectral component, while the ML modes outside stable locking range can be suppressed. For Fig. 4.1 (a), M1 is at longer wavelength than M2's. For Fig. 4.1 (c), M1 is at shorter wavelength than M2's.

On the other hand, Fig. 4.1(b) is the special case that the two MLs are within the locking range of SL. In this case, they can share the power of the SL and significant output powers are produced at both master laser frequencies. In addition to, it is found that the M1 at the longer wavelength (or lower frequency) produces larger optical power than M2 at the shorter wavelength. Fig.4.1 (d) shows when the SL locked to neither of the two MLs. Thus the spectrum has three dominant peaks at each frequency of master

lasers and slave laser frequency.
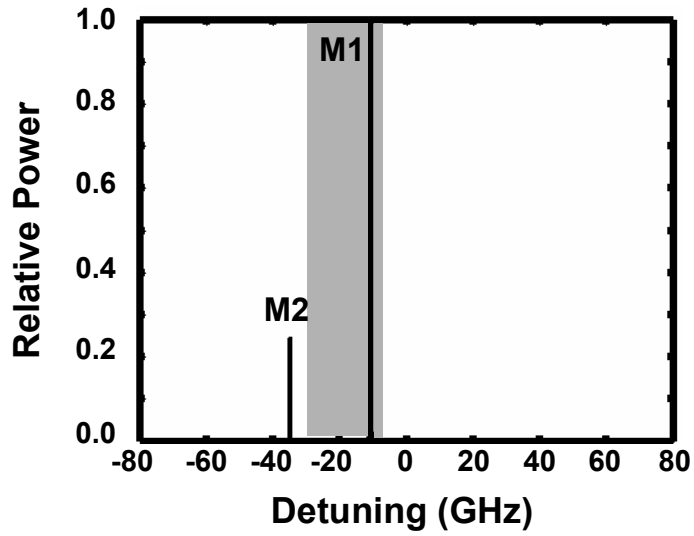
(a)
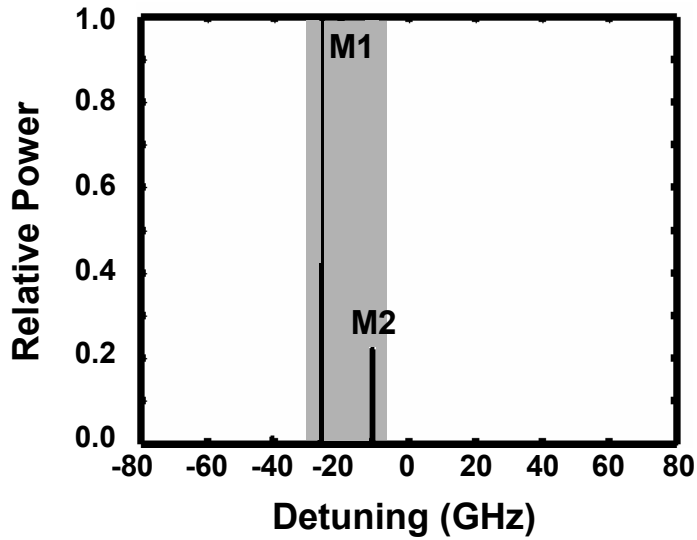
(b)

Figure 4.1 Power spectra at different operating point. M1 represents first master laser, M2 second master laser, and S slave laser.
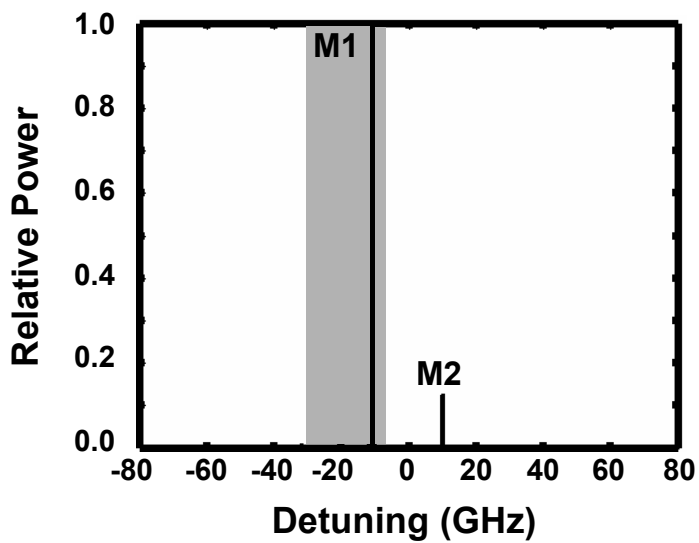
(c)
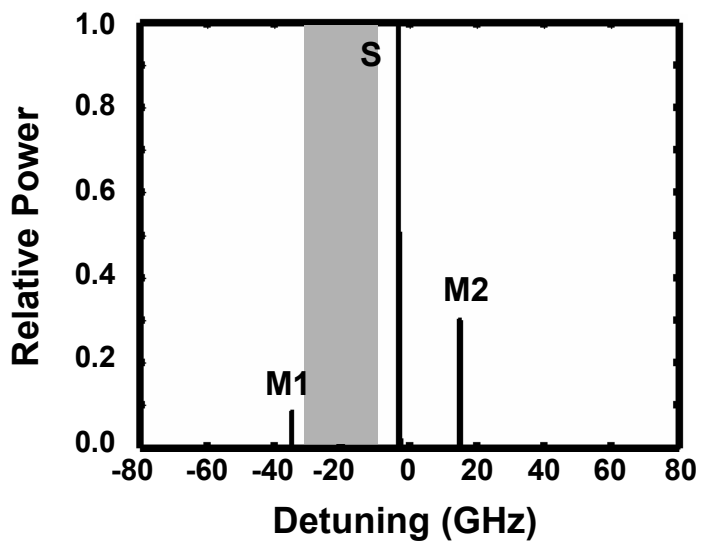
(d)

Figure 4.1 (Continued)

The power sharing characteristics of the two MLs within the locking range is also investigated. Fig. 4.2 is the calculated relative peak power changes of M1 and M2 in the SL power spectra when M1 is fixed at the shorter wavelength (or higher detuning frequency, $\Delta f_{M1} = -8\,GHz$) within locking range and M2 is tuned in wavelength ($-50\,GHz \leq \Delta f_{M2} \leq 40\,GHz$). The shaded area represents the calculated locking range for each ML ($-30\,GHz \leq \Delta f_{Locking\,for\,M1}\,(= \Delta f_{locking\,for\,M2}) \leq -5\,GHz$). The horizontal axis is the detuning frequency of the tuned M2. In this figure, the thin solid line (a) represents the peak power change of the M1 fixed in locking range and the thick solid line (b) represents one of the M2 when the M2 is tuned.

The Region (i) and (iii) correspond to the cases of Fig. 4.1 (a) and Fig. 4.1 (c), respectively. In these regions, only the M1 is within locking range and obtain larger power of the SL than M2 outside locking range. On the other hand, when the M2 is tuned in region (ii) where both M1 and M2 are within locking range, they can share power of the SL, but M2 at longer wavelength (or lower frequency detuning than M1, $\Delta f_{M2} \leq -8\,GHz$) become to larger than the M1. Since the locking range is obtained for only one ML, it cannot exactly expect the region where the two MLs share the power of the SL. However, it clearly shows the tendency of the wavelength dependent power changes between the two MLs near the approximated locking range. This result is related to the asymmetric locked power versus

detuning frequency in section II. Thus, the characteristics of the SL under

external light injection are determined by locking mechanism.
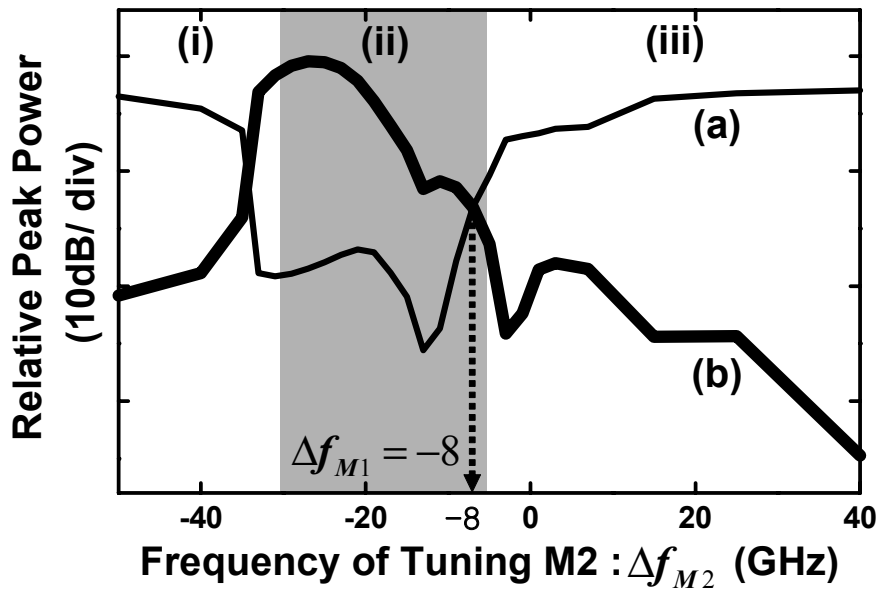
Figure 4.2 Simulated relative peak power changes of the M1 (a) and M2 (b) in SL power spectra when the M1 is fixed ($\Delta f_{M1} = -8\,GHz$) and M2 is tuned ($-50\,GHz \leq \Delta f_{M2} \leq 40\,GHz$).

B. Experiment
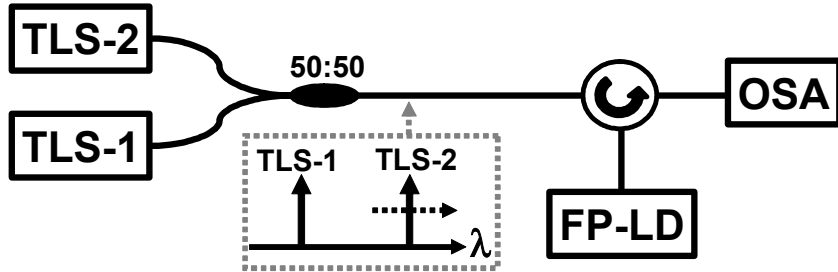
Figure 4.3 Experimental setup for characteristics of the SL under two ML light injections. TLS: tunable light source and OSA: optical spectrum analyzer,

In order to verify the above characteristics of the SL under external light injection, experiment were performed using a Fabry-Perot laser diode (FP-LD) subject to light injections from two tunable light sources (TLSs), having the same amplitude, as shown in Fig. 4.3. The two signals injected to one target mode of FP-LD modes, so the characteristics of a single mode semiconductor laser under several laser can be applied to the FP-LD. As shown in Fig. 4.3, one (TLS-1) of the two TLSs injected to FP-LD is fixed at a wavelength within a locking range and the other (TLS-2) was tuned in the direction of longer wavelength side. In Fig. 4.3, the two thick arrows and the dotted arrow represent tuning TLS, fixed TLS, and tuning direction,

respectively. The bias current is $2 \times I_{th}$ ($I_{th} \approx 5mA$) and the target mode is the peak mode of FP-LD at the wavelength of 1549.37nm.

Fig. 4.4 shows the measured optical peak powers of the FP-LD under the two light injections for three conditions corresponding to Fig. 4.1 (a), (b), and (c). The measured locking range of the FP-LD for one TLS is from 1549.53nm to 1549.67nm in wavelength and illustrated as the shaded area in the figures. First, Fig. 4.4 (a) and (c) show the case of Fig. 4.1 (a) and (c), respectively. The TLS-1 within locking range obtains larger power of the FP-LD and becomes the largest mode in optical spectrum. On the other hand, when the TLS-1 and TLS-2 are within locking range, as shown in Fig. 4.4 (b), they share the power of FP-LD, but TLS-2 at longer wavelength obtained larger power. Therefore, the results confirm that the behavior of the SL under external several light injections is controlled by injection-locking mechanism.
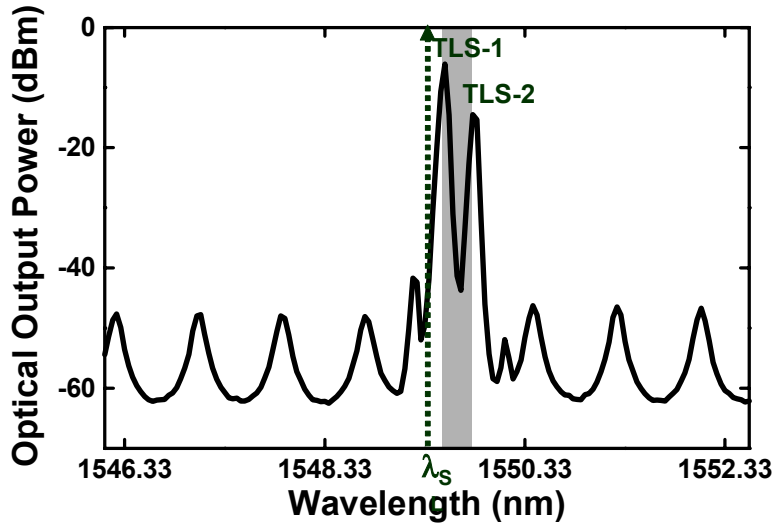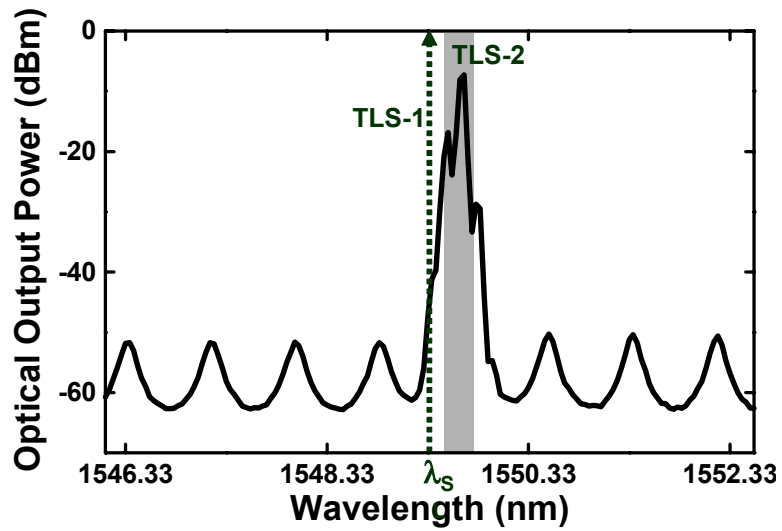
Figure 4.4 Measured optical spectra of the SL under two ML injections for case that only the TLS-1 is within locking range and TLS-2 is outside locking range at longer wavelength than TLS-1's (a) and for the case that TLS-1 and TLS-2 are within locking range (b)
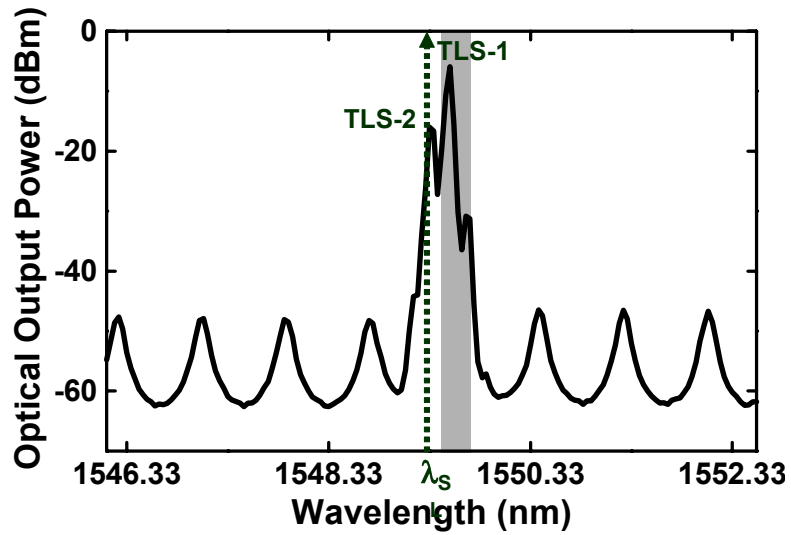
Figure 4.4 Measured optical spectra of the SL under two ML injections for case that only the TLS-1 is within locking range and the TLS-2 is outside locking range at the shorter wavelength than TLS-1's (c).

V. New optical single sideband modulation using a semiconductor laser under modulated light injection

As mentioned before, the intensity modulation has been intensively studied, because of its simplicity to transmit optical signals in RoF system. However, the intensity modulation has two problems: modulation bandwidth limitation and dispersion induced power degradation. Previous methods to overcome these problems have shown successful results, but all of them have been focused to solve only one of the two. Therefore, we proposed the new optical single sideband modulation scheme overcoming modulation bandwidth limitation and chromatic dispersion induced power degradation at the same time. The proposed scheme utilizes a semiconductor laser (SL) under modulated light injection as an optical active filter. This operation is based on wavelength selective amplification characteristics of an SL subject to external light injections, which have been discussed in section III and IV. This section first deals with the operation principle of the proposed scheme. In order to verify the scheme, experiments have been demonstrated. The results shows that the new scheme can overcome dispersion induced power degradation and modulation bandwidth limitation.

A. Operation principle

The conceptual diagram of the proposed scheme is described in Fig. 5.1. An SL under light injection transforms the input DSB signals into SSB signals with the gain and filtering characteristics.
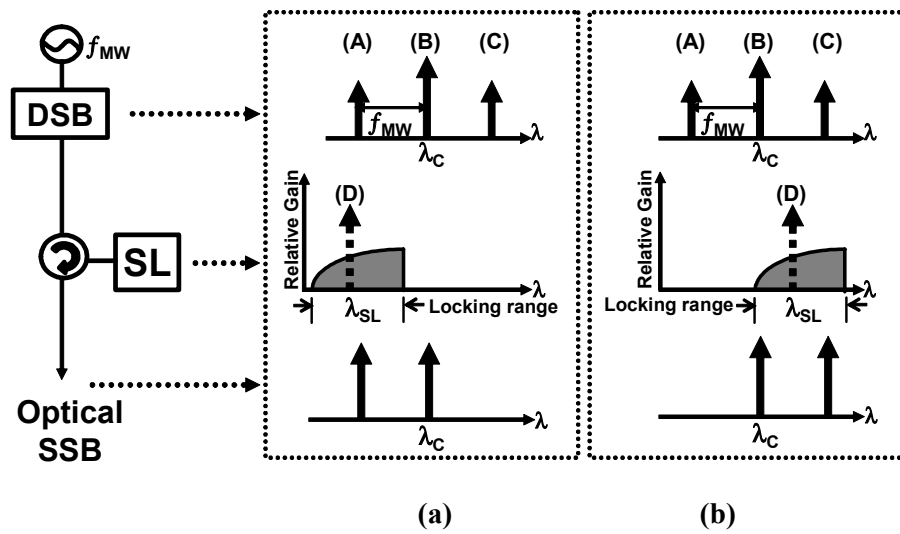
Figure 5.1 Proposed schemes. (a) For the case in which one mode of DSB (A) at the shorter wavelength is within locking range. (b) For the case in which two modes of DSB (B and C) at the longer wavelength are within locking range. SL: Semiconductor laser.

Here, three components of the modulated ML, double sidebands and optical carrier, can be considered as three external lasers injected to the SL. As discussed in section III and IV, when the external ML lights inject to an

SL and any ML modes are within locking range, the SL does not have power at its own free-running frequency but at the ML modes. That is, the ML modes within locking range obtain and share most power of the SL. On the other hand, other modes outside locking range show weak peaks in the power spectrum of the SL. As the result, if we simply consider power relationship of the input ML modes and the output SL modes, the SL can be regarded as an optical band-pass filter with pass-band of locking range. The transfer function of the new filter is not flat within pass-band but wavelength dependent. The input mode at longer wavelength obtains larger band-pass response. Thus, the shape of the band-pass response becomes asymmetric in terms of wavelength (or frequency), as shown in Fig. 5.1.

In addition, the new filter can provide gain, which is defined as the power ratio of the ML mode in output SL to the input ML mode. Since the output SL power is determined by the bias current of SL, under satisfying the wanted filtering condition, higher current of the SL provides larger gain. Therefore, the SL under external light injections can be regarded as an active optical filter with the gain and filtering characteristic of Fig. 5.1. In Fig. 5.1, the free-running (without any injection) SL has the wavelength λ_{SL} represented by dotted arrows (D). The shaded areas represent the relative gain within the locking range that input optical signals will experience.

When one sideband at the shorter wavelength of the DSB signals (A) is

located within the stable locking range as shown in Fig. 5.1 (a), injection locking occurs and this sideband obtains the largest optical gain in the SL. On the contrary, other DSB modes (B and C) outside the locking range become suppressed. Since mode (B) is sufficiently large to start with, two dominants modes (A and B) are realized and the optical SSB generation is achieved. When two or even three DSB optical modes (B and C) are located within the stable locking range as shown in Fig. 5.1 (b), both of them receive gain but the mode (C) at the longer wavelength gets the larger optical gain. Consequently, the optical SSB generation is again achieved.

By amplifying the relatively weak sideband, even when the intensity modulation is performed at high frequency and results in weakly modulated sidebands, the modulation response can be effectively enhanced. In addition, since the relatively excess carrier is suppressed but the weak sideband is enhanced, the effective modulation depth can be increased. This is advantageous, because it leads to a reduction of the RF insertion loss of a link equal to the carrier suppression, if the average optical power level is increased to compensate the attenuation of the carrier.

B. Experiment for single sideband modulation
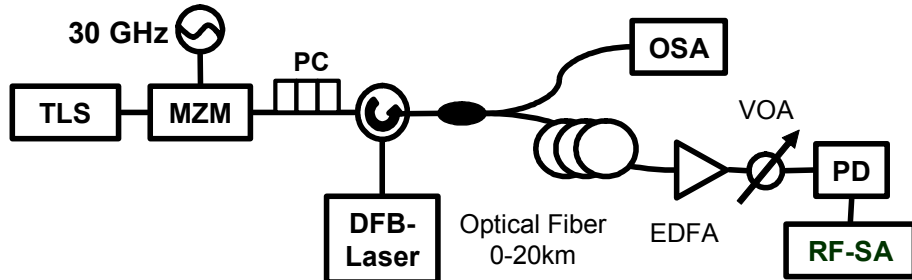
Figure 5.2 Experimental setup for optical single sideband modulation. TLS: tunable light source, MZM: Mach-Zehnder intensity modulator, PC: polarization controller; OSA: optical spectrum analyzer, EDFA: erbium-doped fiber amplifier, VOA: variable optical attenuator, and RF-SA: RF-spectrum analyzer.

First, in order to verify that the proposed concept can overcome the chromatic dispersion induced power degradation, experiments were performed with a setup shown in Fig. 5.2. The intensity modulation at 30 GHz was done by modulating light from a tunable external cavity laser with a 40 GHz Mach-Zehnder intensity modulator. The consequent optical spectrum of intensity modulated ML is shown as input in Fig. 5.3, where each sideband is separated by 30 GHz from the optical carrier. The intensity-modulated light was injected into an unisolated DFB laser diode biased at 12

3 5

mA near the threshold ($I_{th} \cong 11$ mA) to ensure wide locking range. The polarization of the injected light was controlled to be the same as that of the DFB-LD. By controlling the temperature of the SL, its lasing wavelength is brought to the desired locking mode of the input ML. As an example, temperature change of about 5 degrees was required between two conditions shown in Fig. 5.3 (a) and (b). Whether or not the desired modes are located within the locking range was easily determined by the presence of a sharp peak at 30GHz in the RF spectrum of photo-detected signals. Fig. 5.3 (a) and (b) show the measured output optical spectra of the resulting optical SSB signals. In both cases, the desired sidebands for SSB are larger than unwanted sidebands by more than 20 dB.

In order to investigate the effects of fiber chromatic dispersion, photo-detected 30 GHz signal powers were measured as function of fiber transmission length and the results are shown in Fig. 5.4. For the compensation of the optical loss in fiber transmission, an Erbium-doped fiber amplifier and a variable optical attenuator were employed before PD as shown in Fig. 5.2. With the DSB signals only, the signal powers were periodically and greatly suppressed in the RF-spectrum as expected. This can be represented by [15];

$$P_{signal} \propto \cos^2\left(\frac{\pi \lambda_{ML}^2 D L f_{mm}^2}{c} + \arctan(\alpha)\right) \qquad (5.1)$$

where D represents the fiber dispersion, L the fiber length, λ_{ML} the center optical carrier wavelength, f_{mm} the electrical modulation frequency, and α the chirp of the modulator used. The solid line in the figure is obtained from curve-fitting the DSB-modulated signal power measurement results with Eq. 5. On the contrary, the optically SSB modulated signals, whose optical spectra are shown in Fig. 5.3 (a) and (b), are not influenced by fiber dispersion as shown in Fig. 5.4.
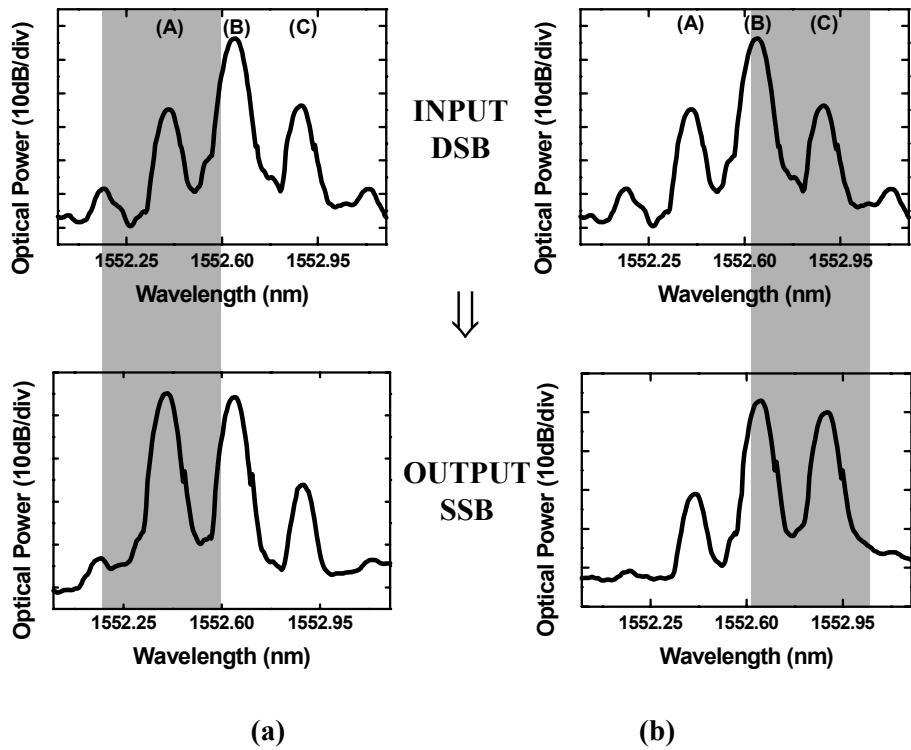
Figure 5.3 Measured optical spectra for input DSB and output optical SSB for the case that one mode of DSB at shorter wavelength (A) is within locking range (a) and for the case that two modes of DSB (B and C) are within locking range (b).
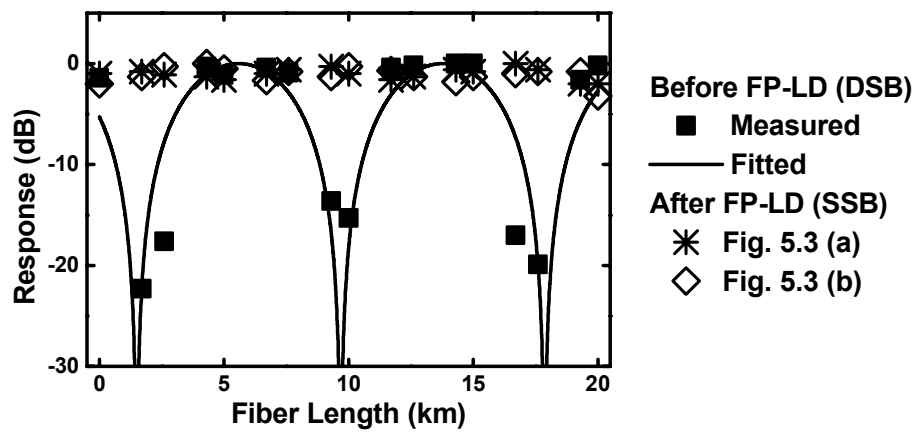
Figure 5.4 Measured RF power versus fiber length

C. Experiment for overcoming modulation bandwidth limitation
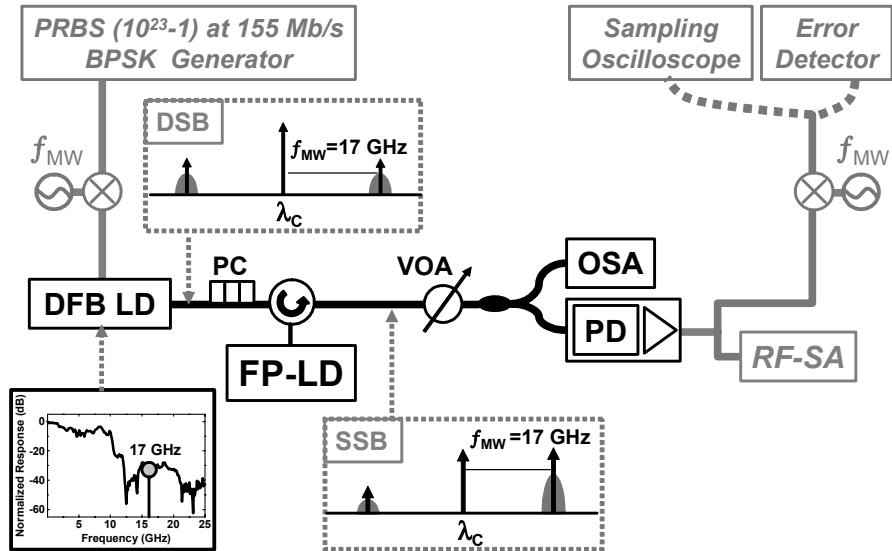
Figure 5.5 Experimental setup for overcoming modulation bandwidth OSA: optical spectrum analyzer, VOA: variable optical attenuator, and RF-SA: RF-spectrum analyzer.

In this part, it is proved that the new scheme overcomes modulation bandwidth limitation by 155 Mb/s BPSK data at 17 GHz transmission experiment. The experimental setup is shown in Fig. 5.5. An Anritsu pattern generator produces a 155 Mb/s nonreturn-to-zero (NRZ) data stream, which is initially mixed with a 17 GHz RF carrier to generate the binary phase-shift

keying (BPSK) data signal. The resulting microwave data signal is then used to directly modulate a single mode laser diode from Lucent, which is commercial for 2.5 Gb/s digital communication with a poor frequency response at 17 GHz. Here, a Fabry-Perot laser diode (FP-LD), biased at 13 mA ($2.6 \times I_{th}$) was used as an active optical filter.

The insets in Fig. 5.6 (a) and (b) show the measured optical spectra for intensity-modulated signals, before and after passing through the FP-LD. Since the resolution of the optical spectrum analyzer available for measurement was not sufficient to clearly resolve the sidebands, a heterodyne spectrum analysis was performed by beating signals of interest (S1, S2, and λ_C) with additional light having λ_{Ex} lower than λ_C by 3 GHz and observing the resulting RF spectrum as schematically shown in Fig. 5.6 (a) and (b). The figure shows the RF spectra, before and after passing through the FP-LD. In the figure, the optical modes that produce the beating signals are identified. As shown in Fig. 5.6 (b), the peak at 20 GHz, corresponding to S2, is larger than the peak at 14 GHz, corresponding to S1, by more than 20 dB, clearly indicating the successful generation of the single sideband spectrum. By amplifying the wanted weakly modulated sideband (S2), optical SSB is generated and the directly photo-detected signal at 17 GHz is clearly enhanced for the generated SSB signal. Therefore, the proposed scheme can overcome the modulation bandwidth limitation.

The down conversion takes place after the photodiode, by mixing the data signal with a 17 GHz local oscillator. The resulting 155 Mb/s data signal may then be displayed on a Tectronics digital sampling oscilloscope for showing eye diagram, or fed into the Anritsu digital data analyzer to determine the bit error rate (BER) of the received signal. We then placed a variable attenuator before the photodiode and measured the received BER as a function of received optical power, with and without passing through the SL. These results are presented in Fig. 5.7 which shows that there is an 11 dB improvement in system performance, for a received BER of 10^{-9}, when the SL filters out unwanted sideband and enhances the wanted sideband. Fig. 5.8 is the eye diagrams of the DSB signal and the generated SSB signal at the received optical power of 7.8 dBm measured by digital sampling oscilloscope. It is obviously shown that the eye for SSB signal is opened. As the results, the proposed scheme overcomes modulation bandwidth limitation by increasing the modulated sidebands effectively.
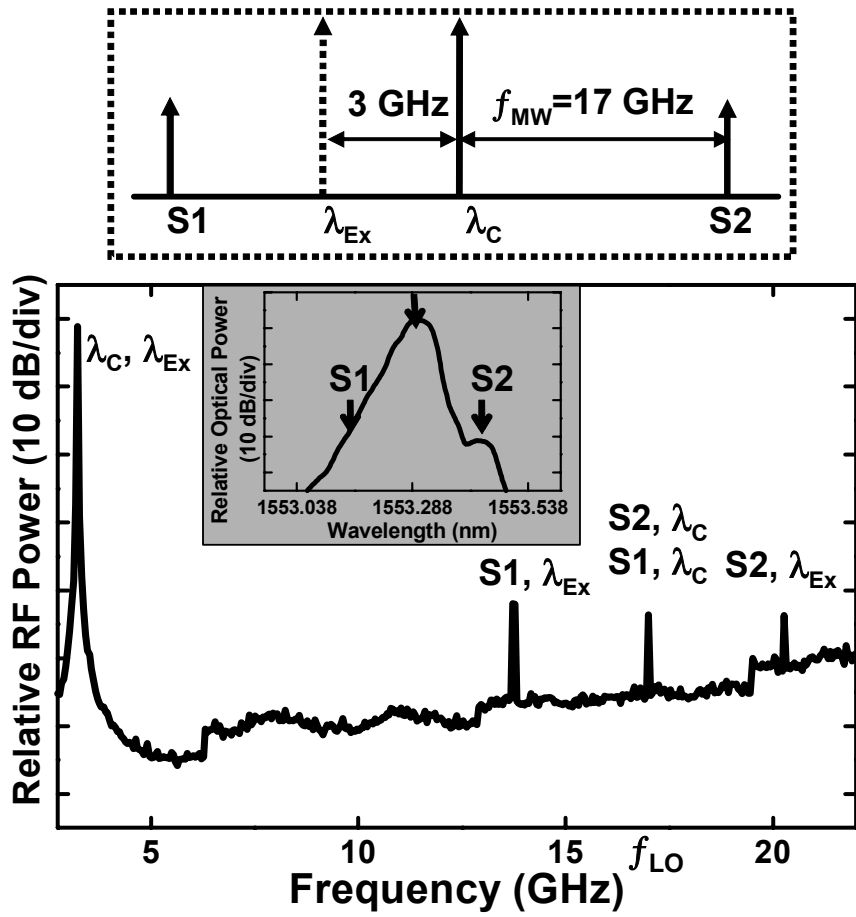
Figure 5.6 Measured optical spectra for DSB before FP-LD (a).
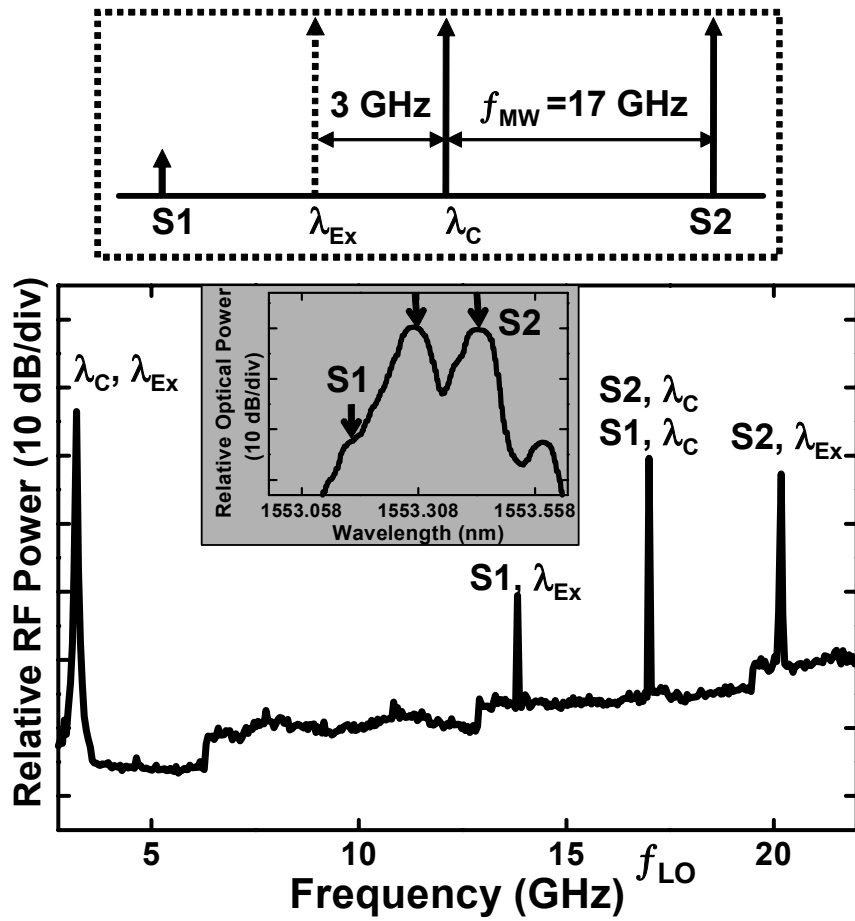
Figure 5.6 Measured optical spectra for SSB after FP-LD (b).
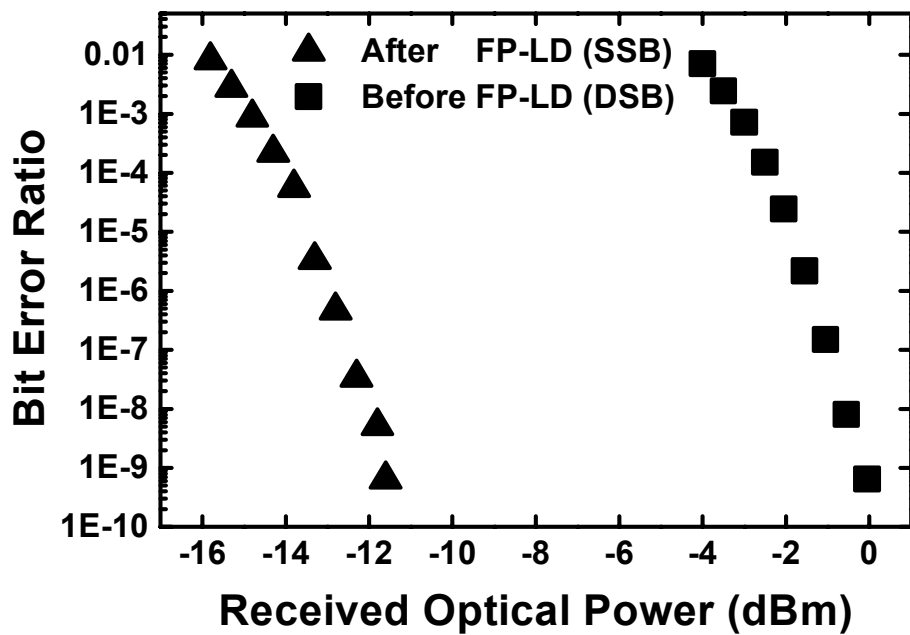
Figure 5.7 Measured Bit Error Rate versus received optical power for DSB signal before FP-LD and for SSB signal after FP-LD.
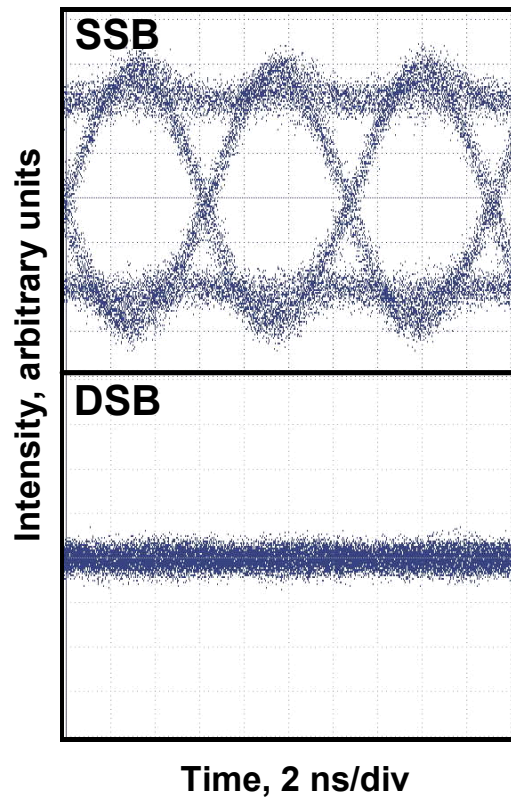
Figure 5.8 Received eye diagrams of 155 Mb/s data signal at the received optical power of 7.8 dBm for DSB signal before FP-LD and for SSB signal after FP-LD.

D. Discussion

Through the above experimental results, the proposed active optical filter is successfully demonstrated. However, there can be some limiting factors and difficulties in proper realization of the scheme. Here, the practical issues are discussed.

In practice, the locking range and relative gain shape of the active optical filter are determined by the wavelength and power of the SL. The wavelength controls the position of locking range in wavelength, leading to the selection of the desired mode. The power controls the width of locking range and relative gain shape. Decrease of the SL power results in the wide locking range, leading to high data rate carrying on the desired sideband. On the other hand, increase of the power brings about the steep slope in the relative gain shape, enabling large suppression ratio of the undesired mode, and large gain, leading to the large modulation bandwidth enhancement. Because of the trade-off between locking range and relative gain shape, the optimal control of the SL power and wavelength is required. Therefore, realization of the active optical filter is dependant on its circumstances such as the injecting ML power, ML's modulation depth, and user's need for data rates and suppression ratio.

For better controllability, large ML power is favorable. The main factor

to lose the injecting input ML power is the poor coupling of the ML to the SL cavity. For the efficient coupling, the polarization of the ML should be the same as that of the SL. Therefore, polarization needs to be controlled carefully.

VI. Conclusion

The intensity modulation is a simple and cost-effective technique to transmit microwave and millimeter wave signals over fiber optic link in radio-on-fiber system. However, the modulation technique has two important problems: modulation bandwidth limitation and chromatic dispersion induced power degradation. In this thesis, the new optical single sideband modulation scheme overcoming both problems simultaneously is proposed and demonstrated experimentally. The proposed scheme employs a semiconductor laser (SL) under external light injection as an active optical filter.

First, the characteristics of the SL under external light injection are discussed, which are the origins of the proposed scheme. For the SL under a single mode master laser (ML), the characteristics are investigated by well-known classical injection locking model. When the ML is within the locking range of the SL, the locking occurs and the ML mode obtains the largest power of the SL. For the SL under several laser injections, simulation with extended rate equations and experiments are performed for analysis. The results show that the ML modes within the locking range of the SL share the power of the SL but the ML mode at longer wavelength obtains the larger power of the SL.

Based on the power spectral analysis of the SL subject to the light injection, its wavelength selective amplification characteristic can be investigated. From the input ML lights and output lights after passing the SL, the SL is considered as an active optical filter. The SL filters out one of the sideband outside the locking range to generate optical single sideband signals and amplifies the weak selected sideband for overcoming modulation bandwidth limitation. In addition to, it suppresses relatively excess optical carrier so that the effective optical modulation depth can be largely increased.

In order to verify the proposed scheme, 30GHz OSSB signals are experimentally generated using a DFB laser diode as the optical filter. The power ratio of the desired sideband to the undesired one was more than 20dB, which is enough value to neglect the dispersion-induced power variation. In the experiment of transmitting 155 Mb/s data over 17 GHz optical microwave signal, the new optical single sideband modulation scheme using Fabry-Perot laser diode provides more than 11 dB improvement in system performance by enhancing modulation response.

Since locking characteristics can be controlled by adjusting SL lasing wavelength and power, the desired filtering and gain characteristics can be easily tuned. The new scheme using a Fabry-Perot laser diode is specially beneficial, not only because it has many modes that can be used for the filtering process so that the wavelength range for this technique can be very

wide but also because it makes the system cost low. Therefore, the proposed scheme to use the favorable Fabry-Perot laser as an active optical filter has potential for the various applications, and this remains as future work.

References

[1] Al-Raweshidy, Hamed. and Komaki, Shozo. *Radio over Fiber Technologies for Mobile Communications Networks*. Boston: Artech House, 2001.

[2] Petermann, Klaus. *Laser diode modulation and noise*. Dordrecht: Kluwer Academic Publishers, 1988.

[3] J. D. Ralston, K. Eisele, R. E. Sah, E. C. Larkins, S. Weisser, J. Rosenzweig, J. Fleissner, and K. Bender, "Low-bias-current direct modulation up to 33 GHz in GaAs-based pseudomorphic MQW ridge-waveguide lasers suitable for monolithic integration," *Semiconductor Laser Conference*, Maui, Hawaii, 14th IEEE International, pp. 211-212, 1994.

[4] S. Weisser, E. C. Larkins, K. Czotscher, W. Benz, D J. aleiden, I. Esquivias, J. Fleissner, J. D. Ralston, B. Romero, R. E. Sah, A. Schonfelder, and J. Rosenzweig, **"**Damping-limited modulation bandwidths up to 40 GHz in undoped short-cavity $In_{0.35}Ga_{0.65}As$-GaAs multiple-quantum-well lasers," *IEEE Photonics Technology Letters*, vol. 8, no. 5, pp. 608-610, 1996.

[5] X. J. Meng, T. Chau, and M. C. Wu, "Experimental demonstration of modulation bandwidth enhancement in distributed feedback lasers with

external light injection," *Electron. Lett.*, vol. 34, no. 21, pp. 2031-2032, 1998.

[6] A. J. Seeds, "Microwave Photonics," *IEEE Trans. Microwave Theory and Tech.*, vol. 50, no. 3, pp. 877-887, 2002.

[7] G. Yabre, "Effect of Relatively Strong Light Injection on the Chirp-to-Power Ratio and the 3dB Bandwidth of Directly Modulated Semiconductor Lasers," *J. Lightwave Technol.*, vol. 14, no. 10, pp.2367-2373, 1996.

[8] T.-D. Ni, X. Zhang, A. S. Dryoush, "Harmonic Enhancement of Modulated Semiconductor Laser with Optical Feedback," *IEEE Microwave Guide Wave Lett.*, vol. 3, no. 5, pp. 139-141, 1993.

[9] H. Toda, Y. Miyazaki, K. Takagi, T. Aouagi, T. Nishimura, and E. Omura, "40 GHz Modulation Bandwidth of Electroabsorption Modulator with narrow-mesa ridge waveguide," in *Optic. Fiber Commun. Conf.*, Anaheim, CA, Tech. Dig., pp. 722-723, 2001.

[10] D. Chen, H. R. Fetterman, A. Chen, W. H. Steier, L. R. Dalton, W. Wang, and Y. Shi, "Demonstration of 110 GHz electro-opti polymer modulators," *Appl. Phys. Lett.*, vol. 70, no. 25, pp. 3335-3337, 1997.

[11] G. L. Li, S. A. Pappert, P. Mages, C. K. Sun, W. S. C. Chang, and P. K. L. Yu, "High-saturation high-speed traveling-wave InGaAsP-InP electroabsorption modulator," *IEEE Photon. Technol. Lett.*, vol. 13, no.

10, pp. 1076-1078, 2001

[12] J. J. O'Relly, P. M. Lane, R. Heidemann, and R. Hofstetter, "Optical generation of very narrow linewidth millimeter-wave signals," Electron. Lett., vol. 28, no. 25, pp. 2309-2311, 1992.

[13] D. G. Moodie, D. Wake, N. G. Walker, and D. Nesset, "Efficient Harmonic Generation Using an Electroabsorption Modulator," *IEEE Photon. Technol. Lett.*, vol. 7, no. 3, pp. 312-314, 1995.

[14] J. Park, W. V. Sorin, and K. Y. Lau, "Elimination of the fibre chromatic dispersion penalty on 1550nm millimetre-wave optical transmission," *Electron., Lett.*, vol. 33, no. 6, pp. 512-513, 1997.

[15] G. H. Smith, D. Novak, and Z. Ahmed, "Overcoming chromatic-dispersion efects in fiber-wireless system incorporating external modulators," *IEEE Trans. Microwave Theory and Tech.*, vol. 45, no. 8, pp. 1410-1415, 1997.

[16] A. Loayssa, D. Benito, and M. J. Garde, "Singel-Sideband Suppressed-Carrier Modulation Using a Single-Electrode Electrooptic Modulator," *IEEE Photon. Technol. Lett*., vol. 13, no. 8, pp. 869-871, 2001.

[17] F. Mogensen, H. Olsen and G. Jacobsen, "Locking Conditions and Stability Properties for a Semiconductor Lasers with External Light Injection,*" IEEE J. Quantum Electron*., vol. 21, no. 7, pp. 784-793, 1985.

[18] R. Lang, "Injection locking properties of a semiconductor laser with external light injection," *IEEE J. Quantum Electron*., vol.18, no. 6, pp. 976-983, 1982.

[19] J. Troger, P.-A. Nicati, L. Thevenaz, and Ph. A. Robert, "Novel Measurement Scheme for Injection-Locking Experiments," *IEEE J. Quantum. Electron*., vol. 35, no. 1, pp. 32-38, 1999.

[20] J. Troger, L. Thevenaz, P.-A. Nicati, and Ph. A. Rober, "Theory and experiment of a single-mode diode laser subject to external light injection from several laser," *J. Lightwave Technol*., vol. 17, no. 4, pp.629-636, 1999.

국 문 요 약

변조된 외부 빛에 주입된 반도체 레이저를 이용한

광학적 Single Sideband 변조

본 논문에서는 크기 변조 방법의 두 가지 문제, 즉 변조 주파수 대역폭 제한과 광섬유의 색분산 영향을 동시에 해결하는 새로운 광학적 single sideband 생성 방법을 제안하였다. 새로운 방법은 간단하게 일반 반도체 레이저를 추가하여 이를 크기 변조된 입력 신호에 대한 광학적 능동 필터로서 이용한다.

빛이 외부에서 들어올 때의 반도체 slave laser (SL) 의 동작 특성을 알아보기 위하여 크게 외부 반도체 master laser (ML) 가 하나일 때와 여럿일 때의 두 가지 경우로 나누어 분석하였다. 먼저 optical injection locking의 수치 해석으로부터, 하나의 ML에 주입된 SL은 ML과 SL의 파워 비와 주파수 차이에 의한 injection locking 영역에 들어온 ML의 주파수에서 파워를 갖는 다는 것을 보였다. 또한, 여러 ML들에 주입된 SL의 특성을 이론적, 실험적 분석을 통하여, 추정된 locking 영역에 들어온 ML들의 주파수에만 SL의 파워가 분포하고, 그 중 낮은 주파수 일수록 (혹은 긴 파장

일수록) 더 큰 파워를 갖는다는 것을 밝혔다. 이와 같은 입력 ML 과 출력 SL의 파워관계로부터. SL이 파장 선택적 증폭 특성을 가진다고 간주할 수 있다.

외부 빛에 주입된 반도체 레이저의 파장 선택적 증폭 특성에 기초하여, 이 레이저가 크기 변조된 입력신호로부터 하나의 선택 안된 sideband 신호를 억제 시켜 single sideband 신호를 생성하고, 선택된 sideband 신호의 크기를 증가시켜서 마치 변조 응답이 강화된 효과를 얻게 한다. 이와 동시에, 상대적으로 과도한 크기의 광 캐리어 신호를 억제함으로써 광변조 지수를 높이는 역할도 할 수 있다.